

Homotopy Analysis Method for Variable Thermal Conductivity Heat Flux Gage with Edge Contact Resistance

Abdul Aziz^a, Farzad Khani^b, and Mohammad Taghi Darvishi^c

^a Department of Mechanical Engineering, School of Engineering and Applied Science, Gonzaga University, Spokane, WA 99258, USA

^b Department of Mathematics, Bakhtar Institute of Higher Education, Ilam, Iran

^c Department of Mathematics, Razi University, Kermanshah 67149, Iran

Reprint requests to F. K.; Fax: +98 841 2238527; farzad_khani59@yahoo.com

Z. Naturforsch. **65a**, 771 – 776 (2010); received October 19, 2009

The homotopy analysis method (HAM) has been used to develop an analytical solution for the thermal performance of a circular-thin-foil heat flux gage with temperature dependent thermal conductivity and thermal contact resistance between the edge of the foil and the heat sink. Temperature distributions in the foil are presented illustrating the effect of incident heat flux, radiation emission from the foil, variable thermal conductivity, and contact resistance between the foil and the heat sink. The HAM results agree up to four places of decimal with the numerical solutions generated using the symbolic algebra package Maple. This close comparison vouches for the high accuracy and stability of the analytic solution.

Key words: Homotopy Analysis Method; Thermal Performance; Heat Flux Gage; Variable Thermal Conductivity; Edge Contact Resistance.

PACS numbers: 44.10.+I; 44.05.+e; 02.60.Lj

1. Introduction

Heat flux gages are widely used in aerospace industry, fire research, measurement of thermophysical properties, and environment monitoring systems [1, 2]. A popular design, the Gardon gage, consists of a thin circular foil of constantan tightly stretched and attached to a copper annulus. The sensing face of the gage is exposed to the heat flux to be measured, while heat transfer from the bottom face is assumed to be negligible. One copper wire is attached to the center of the foil and forms the hot junction. The cold junction is formed by attaching a second copper wire to the copper annulus at the outer edge of the foil. The copper-constantan thermocouple records the temperature difference between the center of the foil and the copper annulus. A calibration graph or an algebraic expression (usually linear) is used to relate the thermocouple output to the measured heat flux. The copper-constantan is the most commonly used combination of metals. The nonlinear mathematical model for the temperature distribution in the foil has been derived by Liechty et al. [3] and Agnone [4]. This model has recently been improved by Aziz and Lopez [5] to include the effects of temperature dependent thermal conduc-

tivity and edge contact resistance. They present three solutions: (i) an exact solution for the zero foil emission, (ii) a perturbation solution when the nonlinearities associated with foil emission and variable thermal conductivity are small, and (iii) direct numerical solutions for the fully nonlinear thermal model with no restriction on the strength of the nonlinear effects. The present paper is contemporaneous with the paper by Aziz and Lopez [5] and uses the homotopy analysis method (HAM) to solve the nonlinear model proposed in [5]. In 1992, Liao proposed a new analytic method for nonlinear problems, namely, the homotopy analysis method [6]. The method does not depend on the presence of small/large parameters in the problem. Furthermore, it can be elegantly combined with many mathematical techniques, such as the Padé method, the numerical methods, and so forth. Especially, unlike other analytic techniques, the homotopy analysis method itself provides a convenient way to control and adjust the convergence of solutions series [7]. Some new solutions have been found by means of the homotopy analysis method [8], which were never reported even by means of numerical techniques. In view of these advantages, the method has been applied to many nonlinear problems [7–18]. In the next section, we

present the solution process for the homotopy analysis method.

2. Nonlinear Heat Flux Gage Model

The nonlinear model governing the temperature distribution in the heat flux gage derived in [5] is

$$\frac{1}{R} \frac{d}{dR} \left[R \frac{d\theta}{dR} (1 + a(\theta - 1)) \right] - A\theta^4 + B = 0. \tag{1}$$

The boundary conditions are

$$R = 0 : \quad \frac{d\theta}{dR} = 0, \tag{2}$$

$$R = 1 : \quad \theta + Rc \frac{d\theta}{dR} (1 + a(\theta - 1)) = 1, \tag{3}$$

where R is the dimensionless radius, θ the dimensionless temperature, A the emission parameter, B the heat flux parameter, a the thermal conductivity parameter, and Rc the contact resistance parameter.

3. Homotopy Analysis Method (HAM)

Let's define the (jointly continuous) map $\Theta(R; q) \mapsto \theta(R)$, where the embedding parameter $q \in [0, 1]$, such that, as q increases from 0 to 1, $\Theta(R; q)$ vary from the initial guess to the exact solution $\theta(R)$. To ensure this, we construct the following zero-order deformation equation of the governing equation:

$$(1 - q)\mathcal{L}[\Theta(R; q) - \theta_0(R)] = \hbar q \mathcal{N}[\Theta(R; q)], \tag{4}$$

where $\hbar \neq 0$ is a convergence-control parameter [10] which helps to ensure the convergence of the solution series; the operator $\mathcal{N}[\Theta(R; q)]$ is defined by the governing equation (1) depending on the two-dimensional case. So \mathcal{N} can be expressed by

$$\mathcal{N}[\Theta(R; q)] := (1 - a) \frac{\partial^2 \Theta}{\partial R^2} + a \left(\Theta \frac{\partial^2 \Theta}{\partial R^2} + \left(\frac{\partial \Theta}{\partial R} \right)^2 \right) - A\Theta^4 + B. \tag{5}$$

The boundary conditions (2) and (3) now yield

$$\begin{aligned} \frac{\partial \Theta}{\partial R}(0; q) &= 0, \\ \Theta(1; q) + Rc \frac{\partial \Theta}{\partial R}(1; q)(1 + a(\Theta(1; q) - 1)) &= 1. \end{aligned} \tag{6}$$

\mathcal{L} is an auxiliary linear operator defined by

$$\mathcal{L}(\Theta) := \frac{\partial^2}{\partial R^2} \Theta. \tag{7}$$

Clearly, when $q = 0$ the zero-order deformation equation (4) and (6) give rise to

$$\Theta(R; 0) = \theta_0(R). \tag{8}$$

When $q = 1$, they become

$$\Theta(R; 1) = \theta(R). \tag{9}$$

Here, $\theta_0(R)$ is the initial guess. We can assume the initial guess of $\theta(R)$ to be

$$\theta_0(R) = \gamma,$$

where $\gamma > 0$ is a constant to be determined by the second equation in (6). Expanding $\Theta(R; q)$ in the Maclaurin series with respect to the embedding parameter q , we obtain

$$\Theta(R; q) = \theta_0(R) + \sum_{k=1}^{\infty} \theta_k(R) q^k, \tag{10}$$

where

$$\theta_k(R) = \frac{1}{k!} \frac{\partial^k}{\partial q^k} \Theta(R; 0). \tag{11}$$

Assuming that above series converges at $q = 1$, we have

$$\theta(R) = \theta_0(R) + \sum_{k=1}^{\infty} \theta_k(R). \tag{12}$$

Differentiating the zero-order deformation equation (4) and (6) m times with respect to q , then setting $q = 0$, and finally dividing by $m!$, we have the high-order deformation equations ($m \geq 1$)

$$\mathcal{L}[\theta_m - \chi_m \theta_{m-1}] = \hbar \mathcal{K}_m \tag{13}$$

with the boundary conditions

$$\begin{aligned} \theta'_m(0) &= 0, \\ \theta_m(1) + Rc \theta'_m(1)(1 + a(\theta_m(1) - 1)) &= 0, \end{aligned} \tag{14}$$

where

$$\chi_m = \begin{cases} 0, & m = 1, \\ 1, & m > 1, \end{cases} \tag{15}$$

and

$$\mathcal{K}_m = (1 - a)\theta''_{m-1} + a \left(\sum_{i=0}^{m-1} \theta''_i \theta_{m-1-i} + \theta'_i \theta'_{m-1-i} \right) - A \sum_{k=0}^{m-1} \theta_k \sum_{i=0}^{m-1-k} \theta_i \sum_{j=0}^{m-1-k-i} \theta_j \theta_{m-1-k-i-j} + B(1 - \chi_m), \tag{16}$$

where the prime denotes differentiation with respect to the similarity variable R . Then the solutions for (13) can be expressed by

$$\theta_m(R) = \chi_m \theta_{m-1}(R) + \hbar \int_0^R d\omega \int_0^\omega \mathcal{K}_m dR + c_1 R + c_2, \tag{17}$$

where the integral constants $c_2 = 0$ and c_1 are determined by the first equation in the boundary conditions (14). Hence, the m th-order approximation of $\theta(R)$ can be generally expressed by

$$\theta_m(R) = \sum_{n=0}^m \Gamma_{m,n}(\hbar) R^{2n}, \tag{18}$$

where $\Gamma_{m,n}(\hbar)$ are dependent upon \hbar . (18) is a family of solutions which is expressed by the auxiliary parameter \hbar . For example, we have

$$\begin{aligned} \theta_1(R) &= R^2 \left(\frac{B\hbar}{2} - \frac{1}{2}A\hbar\gamma^4 \right), \\ \theta_2(R) &= R^2 \left(\frac{B\hbar}{2} + \frac{B\hbar^2}{2} - \frac{1}{2}aB\hbar^2 + \frac{1}{2}aB\hbar^2\gamma \right. \\ &\quad \left. - \frac{1}{2}A\hbar\gamma^4 - \frac{1}{2}A\hbar^2\gamma^4 + \frac{1}{2}aA\hbar^2\gamma^4 - \frac{1}{2}aA\hbar^2\gamma^5 \right) \\ &\quad + R^4 \left(-\frac{1}{6}AB\hbar^2\gamma^3 + \frac{1}{6}A^2\hbar^2\gamma^7 \right). \end{aligned}$$

With the aid of mathematical software, such as Mathematica or Maple, it is easy to proceed to high orders.

4. Results and Discussion

Note that, right now, there are still two parameters γ and \hbar that are unknown. The parameter $\gamma > 0$ is determined by imposing the second boundary condition given by (6). The Newton-Raphson method may be used in evaluating the value of γ . It is important to ensure that the solution series (12) converges. Fortunately, we have the freedom to choose the values of the

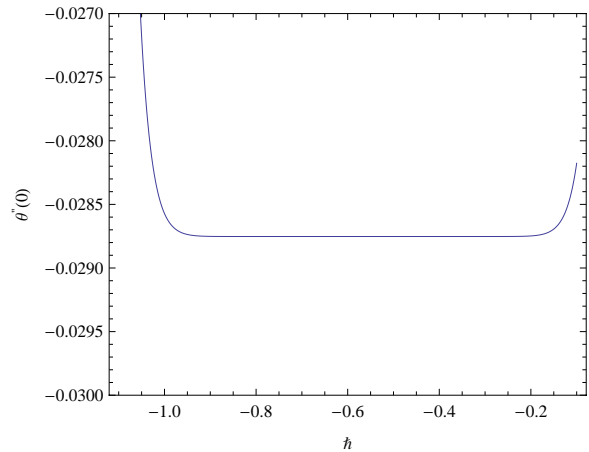


Fig. 1 (colour online). $\theta''(0)$ versus \hbar for the 20th-order approximation at $a = 1$, $Rc = 3$, $A = 1$, and $B = 10$.

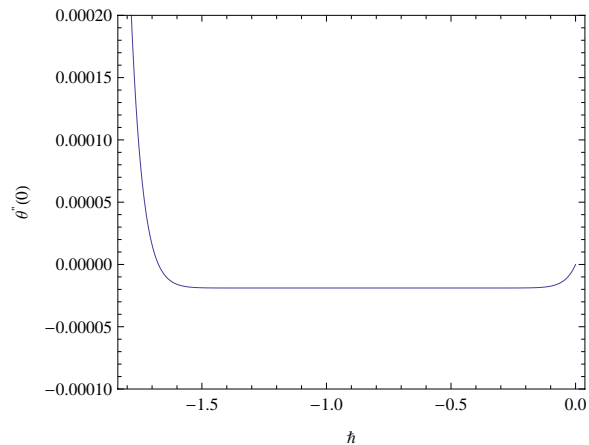


Fig. 2 (colour online). $\theta''(0)$ versus \hbar for the 20th-order approximation at $a = 0.25$, $Rc = 1$, $A = 10$, and $B = 100$.

auxiliary parameter \hbar . This parameter provides a simple way to adjust and control the convergence region and as well as the rate of convergence of the series solution, as shown by Liao [6]. Let \hbar be an unknown variable. By plotting the curves of $\theta''(0)$ versus \hbar , it is possible to choose the proper values of \hbar so as to ensure that the series solution converges. A sample of these calculations is shown in Figures 1 and 2. It can be observed that \hbar must be negative. When $A = B$, the exact solution of (1) with the boundary conditions (2) and (3) is $\theta(R) = 1$. We managed to obtain this result using HAM, too. In order to compare the HAM results with the direct numerical results, the problem was solved using the symbolic algebra package Maple 13. The numerical solution is implemented by calling the proce-

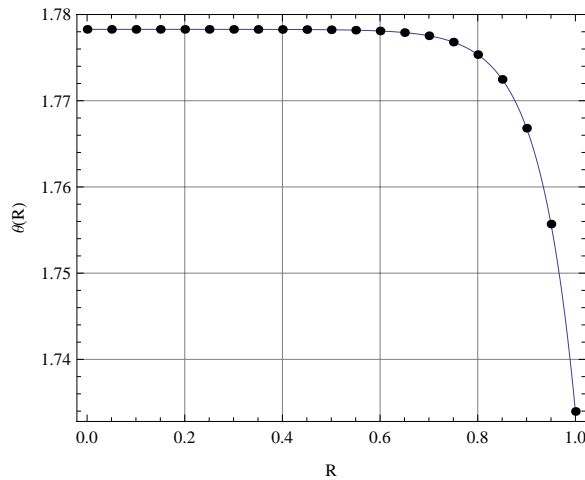


Fig. 3 (colour online). Comparison of the numerical result with analytic approximation when $a = 0.25$, $Rc = 1$, $A = 10$, and $B = 100$. Solid line: 20th-order HAM approximation; filled circle: numerical result.

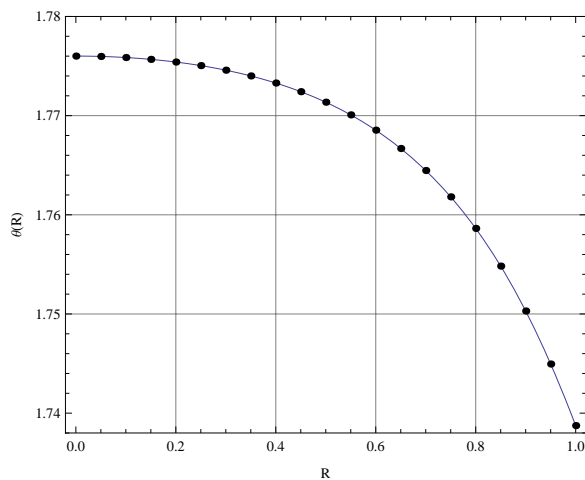


Fig. 4 (colour online). Comparison of the numerical result with analytic approximation when $a = 1$, $Rc = 3$, $A = 1$, and $B = 10$. Solid line: 20th-order HAM approximation; filled circle: numerical result.

procedure 'dsolve' (differential equation solver). Maple offers a choice of methods for use with the numeric option. The method chosen for the numerical integration was 'midrich' (midpoint method with Richardson extrapolation). This method led to a faster convergence and produced stable solutions for all parametric studies performed.

Because of the presence of four independent parameters in the problem, namely, A , B , a , and Rc , it is not practical to present the results for all feasible combi-

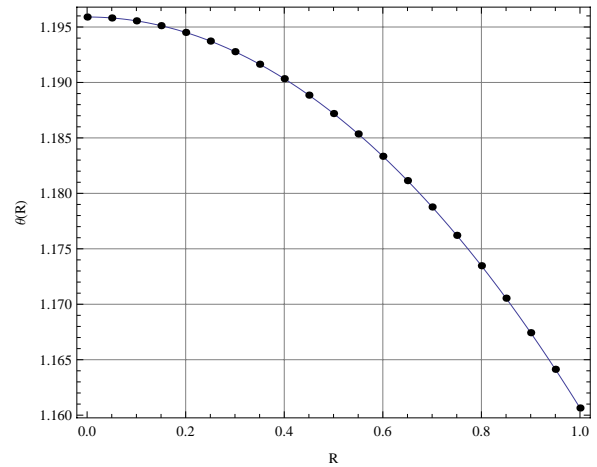


Fig. 5 (colour online). Comparison of the numerical result with analytic approximation when $a = 0.75$, $Rc = 2$, $A = 0.01$, and $B = 0.1$. Solid line: 20th-order HAM approximation; filled circle: numerical result.

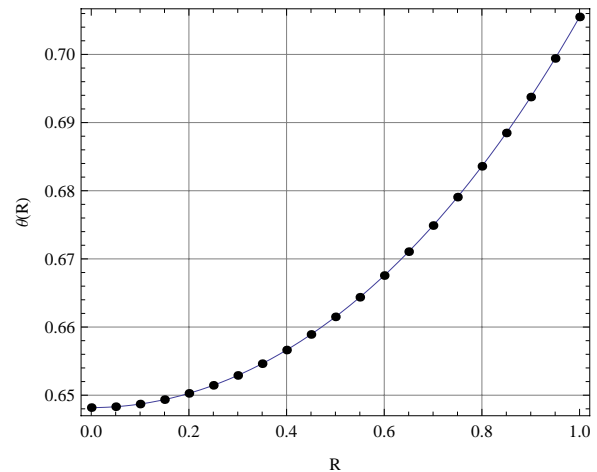


Fig. 6 (colour online). Comparison of the numerical result with analytic approximation when $a = 0.75$, $Rc = 3$, $A = 1$, and $B = 0.1$. Solid line: 20th-order HAM approximation; filled circle: numerical result.

nations of the parameters. Thus, only a selection of results is presented to demonstrate the efficacy of HAM. Figure 3 gives the temperature distribution in the foil for $a = 0.25$, $Rc = 1$, $A = 10$, and $B = 100$. The numerical results delivered by Maple are indicated by solid dots. The agreement between the HAM and the Maple results is excellent. In fact, the two results in every case investigated agreed to at least four places of decimal. Since the incident heat flux is ten times the foil emission, the foil gains energy on the net. This energy is conducted radially along the foil and deposited into the

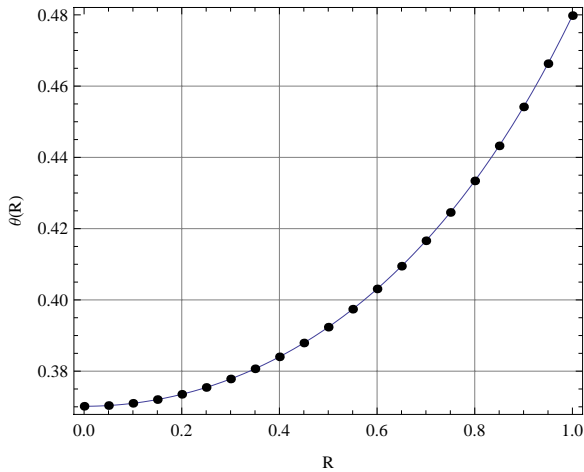


Fig. 7 (colour online). Comparison of the numerical result with analytic approximation when $a = 0.75$, $Rc = 3$, $A = 10$, and $B = 0.1$. Solid line: 20th-order HAM approximation; filled circle: numerical result.

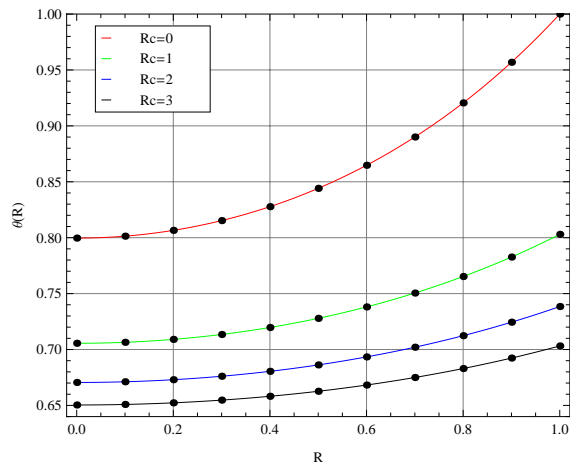


Fig. 8 (colour online). Comparison of the numerical results with analytic approximations when $a = 0.5$, $A = 1$, and $B = 0.1$ for different values of Rc . Solid line: 20th-order HAM approximations; filled circle: numerical results.

heat sink at the edge ($R = 1$). The maximum temperature occurs at the center of the foil. Figure 4 for which $a = 1$, $Rc = 3$, $A = 1$, and $B = 10$ exhibits a pattern similar to Figure 3 because the incident heat flux in this case is also ten times the foil emission. Figure 5 illustrates the temperature distribution when both the incident heat flux and the emission are relatively weak. Since the incident heat flux is still ten times the emission, the curve retains the patterns of Figures 3 and 4, but the temperature at the center of the foil as well as the temperatures throughout the foil are considerable

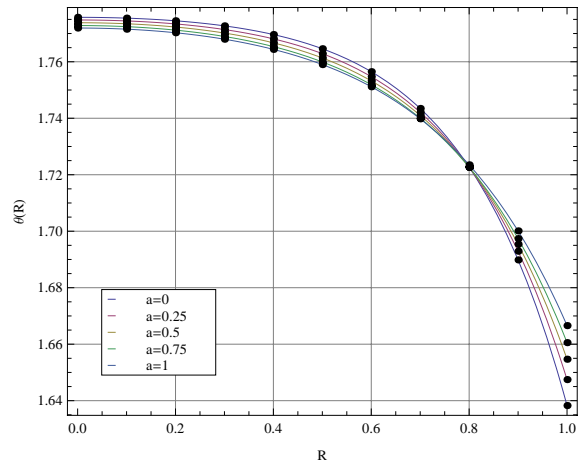


Fig. 9 (colour online). Comparison of the numerical results with analytic approximations when $Rc = 1$, $A = 1$, and $B = 10$ for different values of a . Solid line: 20th-order HAM approximation; filled circle: numerical results.

reduced due to the weak incident heat flux. When the emission from the foil exceeds the incident heat flux, the heat sink supplies the deficit energy to the foil. This can be seen in the temperature profile depicted in Figure 6 which corresponds to $A = 1$, $B = 0.1$, $a = 0.75$, and $Rc = 3$. It may be noted that now the emission is ten times the incident heat flux. The temperature decreases from the edge of the foil to the center of the foil indicating the flow of heat from sink to the foil. Further reductions in temperatures are manifested when the emission is increased to hundred times the incident flux as shown in Figure 7. Figure 8 has been prepared to demonstrate the effect of contact resistance on the temperature distribution in the foil. The parametric values chosen are $a = 0.5$, $A = 1$, $B = 0.1$. The highest temperatures are encountered when the contact resistance $Rc = 0$. As Rc increases the temperatures in the foil decrease progressively so does the temperature drop from the edge of the foil to the center. The biggest temperature drop occurs when $Rc = 0$. The temperature drop becomes smaller as Rc increases and is the smallest when $Rc = 3$. An interesting interplay between the effect of variable thermal conductivity and the effect of contact resistance was observed in the temperature distribution in the foil. A sample of this interplay is illustrated in Figure 9 for $A = 1$, $B = 10$, and $Rc = 1$. As the thermal conductivity parameter a increases, the temperature in the foil decreases but at a certain radial location R , this trend is reversed as the curves crossover. The reversal occurs between $R = 0.8$ and $R = 1$ depending on the value of the parameter a . From a phys-

ical perspective, the effect of an increase in thermal conductivity with temperature should be to lower the temperature and the effect of contact resistance should be to elevate the temperature in the foil. The competition between these opposing effects is exhibited in Figure 9. In the high temperature region, that is, the region between $R = 0$ and 0.8, the increase of thermal conductivity with temperature exerts a greater influence on the temperature distribution than the effect of contact re-

sistance. However, in the low temperature region, that is, in the region R between 0.8 and 1.0, the influence of contact resistance prevails over the influence of thermal conductivity variation and, hence, the reversal-of-trend noted earlier.

Acknowledgement

This work is partly supported by Bakhtar Institute of Higher Education of Iran.

- [1] E. F. Diller, *Advances in Heat Flux Measurements*, *Advances in Heat Transf.*, edited by J. P. Hartnett, T. F. Irvine, Jr., and Y. I. Cho, Vol. 21, Academic Press, Boston 1993.
- [2] N. R. Keltner, *Heat Flux Measurements: Theory and Applications*, Chapter 8 in *Thermal Measurements in Electronics Cooling*, ed. K. Azar, CRC Press, New York 1997.
- [3] B. C. Liechty, M. M. Clark, and M. R. Jones, *J. Thermophys. Heat Transf.* **21**, 468 (2007).
- [4] A. M. Agnone, *J. Thermophys. Heat Transf.* **23**, 33 (2009).
- [5] A. Aziz and R. N. Lopez, *AIAA J. Thermophys. Heat Transf.* (submitted).
- [6] S. J. Liao, *Beyond perturbation: introduction to the homotopy analysis method*, Chapman & Hall/CRC Press, Boca Raton 2003.
- [7] S. Liang and D. J. Jeffrey, *Commun. Nonlinear Sci. Numer. Simul.* **14**, 4057 (2009).
- [8] S. J. Liao and E. Magyari, *Z. Angew. Math. Phys.* **57**, 777 (2006).
- [9] S. J. Liao and Y. Tan, *Stud. Appl. Math.* **119**, 297 (2007).
- [10] S. J. Liao, *Commun. Nonlinear Sci. Numer. Simul.* **14**, 983 (2009).
- [11] A. Molabahrami and F. Khani, *Nonlinear Anal. Real World Appl.* **10**, 589 (2009).
- [12] F. Khani, M. Ahmadzadeh Raji, and S. Hamed-Nezhad, *Commun. Nonlinear Sci. Numer. Simul.* **14**, 3007 (2009).
- [13] F. Khani, A. Farmany, M. Ahmadzadeh Raji, A. Aziz, and F. Samadi, *Commun. Nonlinear Sci. Numer. Simul.* **14**, 3867 (2009).
- [14] F. Khani, M. Ahmadzadeh Raji, and H. Hamed-Nejad, *Commun. Nonlinear Sci. Numer. Simul.* **14**, 3327 (2009).
- [15] F. Khani and A. Aziz, *Commun. Nonlinear Sci. Numer. Simul.* **15**, 590 (2010).
- [16] M. T. Darvishi and F. Khani, *Comput. Math. Appl.* **58**, 360 (2009).
- [17] A. Aziz and F. Khani, *Commun. Nonlinear Sci. Numer. Simul.* **15**, 1565 (2010).
- [18] S. J. Liao, *Int. J. Heat Mass Transf.* **48**, 2529 (2005).